Wegener Center for Climate and Global Change
University of Graz
Leechgasse 25, A-8010 Graz, Austria

Atmospheric Remote Sensing and Climate System Research Group
MULTICLIM Project Report

WegCenter/UniGraz Technical Report for FFG-ALR No. 2/2007

FFG-ALR Study:

MULTICLIM – From CHAMP towards Multi-Satellite Climate Monitoring based on the METOP and COSMIC Missions

[Contract No: ALR-OEWP-WV-326/06 – March 2006]

Enhancement Report
[WP2: ADVANCE]

Advanced retrieval of atmospheric profiles and SST from IASI data

M. Schwaerz, M. Pock, and G. Kirchengast

Wegener Center for Climate and Global Change (WegCenter),
University of Graz, Graz, Austria

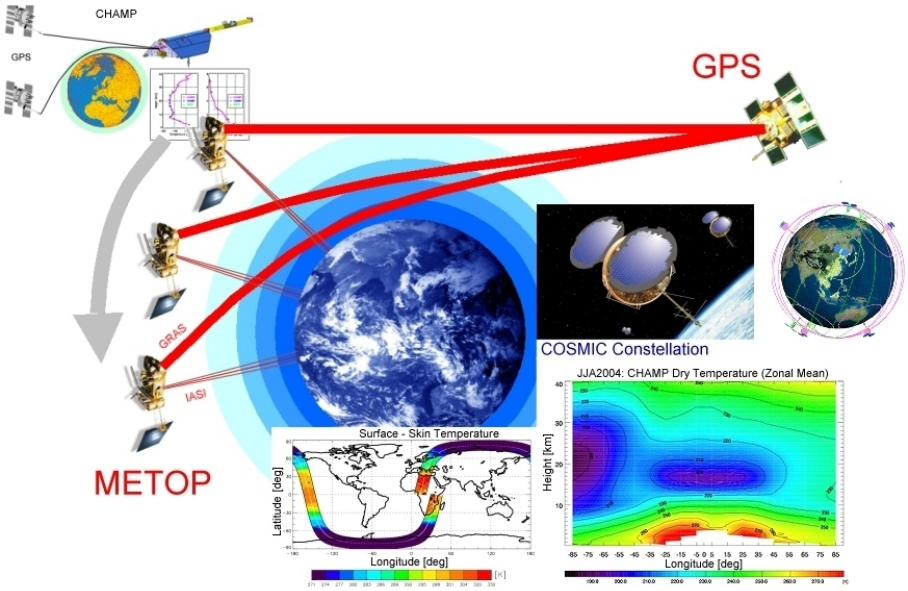

April 2007

Contents

List of Abbreviations

Acronym	Description
CIRA	COSPAR International Reference Atmosphere
COSPAR	Committee on Space Research
CNES	Centre National d'Etudes Spatial
CPU	Central Processing Unit
ECMWF	European Centre for Medium-Range Weather Forecasts
EGOPS	End-to-end GNSS Occultation Performance Simulator
ENVISAT	Environmental Satellite
ESA	European Space Agency
EUMETSAT	European Organisation for the Exploitation of Meteorological Satellites
FTC	Fast Transmittance Coefficient
FWHM	Full Width at Half Maximum
GNSS	Global Navigation Satellite System
GPS	Global Positioning System
IASI	Infrared Atmospheric Sounding Interferometer
IC	Information Content
IR	Infrared
ISRF	Instrument Spectral Response Function
METOP	Meteorological Operational (Satellite)
MS	Maximum Sensitivity
NWP	Numerical Weather Prediction
pdf	probability density function
RMS	Root Mean Square
RO	Radio Occultation
RT	Radiative Transfer
RTIASI	Radiative Transfer Model for IASI
SAT	Surface Air Temperature (2 m Temperature)
SNR	Signal-to-noise Ratio
SST	Surface Skin Temperature; Sea Surface Temperature
UTC	Coordinated Universal Time

Table 1: The Table contains the relevant acronyms used in the current work.

1 Introduction

The overarching goal of MULTICLIM is to prepare for global monitoring of the climate evolution of the upper troposphere/lower stratosphere region with unprecedented accuracy and consistency and thereby help to improve the ability to detect, attribute, and predict climate variability and change. The key datasets for this purpose are RO data and IASI interferometer data, of which the latter are in the focus of the MULTICLIM project.

The IASI (Infrared Atmospheric Sounding Interferometer – see, e.g. *Camy-Peyret and Eyre* (1998), *Weisz* (2001), http://smsc.cnes.fr/IASI/) instrument is part of the core payload of the MetOp series of polar-orbiting operational meteorological satellites currently prepared for EUMETSAT where the first satellite, MetOp-A was successfully launched on Oct. 19, 2006. IASI is a Michelson-type Fourier transform interferometer which samples a part of the infrared (IR) spectrum contiguously from 645 cm^{-1} to 2760 cm^{-1} ($\sim$3.6 μm - 15.5 μm) with an unapodized spectral resolution of about 0.5 cm^{-1}.

The project aims at advancing IASI retrieval algorithms and at preparing IASI climatology processing for climatologies at high horizontal resolution, but also with horizontal gridding matching RO climatologies prepared in parallel in a separate project. The retrieved IASI temperature and humidity profiles and IASI sea surface temperature (SST) will be validated against analysis fields from ECMWF.

In particular, the main goals of this report is the setup of an advanced retrieval processing system for atmospheric profiles (temperature, humidity, ozone), and SST from IASI data.

Temperature profiles are obtained from observations in the absorption bands of carbon dioxide (CO_2), which is a relatively abundant trace gas of known and uniform distribution. Other atmospheric constituents absorbing in the thermal IR are H_2O (water vapor and temperature sounding), O_3 (ozone profiling), N_2O, CH_4, and CO (trace gas column amounts). The atmospheric window regions, where attenuation is minimal, are used to obtain surface and cloud properties. With the opportunity of a very high spectral resolution at several wavelengths, the possibility of observing different height layers can be established by taking into account that radiances measured near the center of an absorption band arise from the upper atmospheric layers, while measurements at the wings of a band will sense deeper into the atmosphere.

One of the primary objectives of the IASI instrument, according to the IASI science plan (*Camy-Peyret and Eyre* (1998)), is the improvement of the vertical resolution of temperature and water vapor profiles to about 1 km in the middle and lower troposphere as well as improving the retrieval accuracy to within 1 K in temperature and $\sim$10% in humidity. A main scientific motivation of this is based on the key role of water vapor in the upper troposphere and its effects on the global climate since only small changes in humidity and its trends have serious implications on the amount of thermal energy escaping to space (*Schmetz et al.* (1995); *Spencer and Braswell* (1997)). Additionally, this level of performance will greatly assist numerical weather prediction (NWP) in delivering accurate and frequent temperature and humidity profiles for operational and research needs and it will supply more accurate quantifications of climate variability, particularly contributing to our knowledge of the climate of the upper troposphere.

In this report a joint temperature, humidity, ozone, and sea surface temperature (more precisely, the surface skin temperature of the ocean) retrieval combined with an efficient channel selection method is introduced and demonstrated. Additionally, a careful error analysis and characterization of the retrieved profiles is given. Section 2 describes the setup of the retrieval processing system introducing the forward model, the retrieval algorithm, and the error characterization functions. In addition, the design of the error covariance matrices and the channel selection algorithms are described. In section 3 the simulation setup is described and the retrieval performance results are discussed, including different channel selection methods, the error analysis and characterization of special profiles, and the comparison of the joint retrieval setup

with single profile retrievals. Finally, section 4 presents a summary and the main conclusions of the report and an outlook to the next steps of work.

2 Joint Retrieval Processing System

In order to successfully retrieve the physical state of the atmosphere – temperature and humidity profiles, etc. – from radiance measurements based on high resolution instruments like IASI a proper modeling of the radiative transfer through the atmosphere is essential which is the forward modeling component of the processing system. The approach we chose to solve this inverse problem is the optimal estimation methodology which constitutes a statistically optimal fusion of imperfect (i.e., noisy) but unbiased measurements and (also imperfect) *a priori* knowledge on the state variables of interest. An instructive and detailed description of this method was given by *Rodgers* (2000).

2.1 Forward Modeling

The state of a physical system, $\mathbf{x}$ (temperature profile, humidity profile, etc.), can be related to measurements, $\mathbf{y}$ (IASI radiance spectra or brightness temperatures, respectively), via a forward model (function), $\mathbf{f}$, by:

$$\mathbf{y} = \mathbf{f}(\mathbf{x}) + \boldsymbol{\epsilon}, \tag{1}$$

where $\boldsymbol{\epsilon}$ is the measurement noise. Since we have to deal with unbiased measurements this measurement error is supposed to be known in terms of systematic biases and random instrument noise – in fact, the measurements $\mathbf{y}$ need be corrected for biases before using them in the retrieval which enables a statistically adequate characterization of $\boldsymbol{\epsilon}$ by a measurement error covariance matrix (see section 2.2). The IASI retrieval problem is moderately nonlinear only (*Lerner et al.* (2002)), i.e., (1) can be approximated by a Taylor series expansion to first order:

$$\mathbf{y} = \mathbf{f}(\mathbf{x}_0) + \mathbf{K}_0(\mathbf{x} - \mathbf{x}_0) + \mathrm{O}\left((\mathbf{x} - \mathbf{x}_0)^2\right) + \boldsymbol{\epsilon}, \tag{2}$$

where $\mathbf{x}_0$ is a suitable reference state and $\mathbf{K}_0 = \partial\mathbf{f}/\partial\mathbf{x}|_{\mathbf{x}=\mathbf{x}_0}$ is the so called weighting function or Jacobian matrix (later denoted by $\mathbf{K}$). The rows of $\mathbf{K}$, each related to a specific element of $\mathbf{y}$, are termed weighting functions.

2.1.1 RTIASI

For the simulation of the IASI measurements (i.e., brightness temperatures $\mathbf{T}_B$) as well as the calculation of the Jacobian matrices for temperature (including surface temperature), humidity, and ozone – $\partial\mathbf{T}_B/\partial\mathbf{T}$, $\partial\mathbf{T}_B/\partial\mathbf{q}$, $\partial\mathbf{T}_B/\partial\mathbf{O}_3$, $\partial\mathbf{T}_B/\partial\mathbf{SST}$ – the fast radiative transfer model RTIASI version 1 (*Matricardi and Saunders* (1999)) was utilized. Briefly speaking, RTIASI-1 provides fast transmittance coefficients (FTC) which have been computed for a set of atmospheric profiles representing the range of variations in temperature and absorber amount found in the real atmosphere. The model calculates $\mathbf{T}_B$ and the Jacobians for the diverse atmospheric profiles (temperature, humidity, and ozone) on 43 pressure levels, from ∼0.1 hPa (which corresponds approximately to a height of 85 km) to surface. All other gases (such as CO_2, N_2O, CO, CH_4, N_2, O_2, HNO_3, OCS, CCL_4, CF_4, CCl_3F (CFC-11) and CCl_2F_2 (CFC-12)) are assumed to be constant in time and space, and are thus called *fixed gases*. The FTC's are then used to calculate optical depths (and transmittances) for any desired input profile. Having them, radiances and brightness temperatures, respectively, are calculated via the solution of the radiative transfer equation.

To obtain quasi-realistic measurements we have to add an additional noise term, $\boldsymbol{\epsilon}$ (c.f. Eq. 1). The noise is modeled (c.f. *Weisz* (2001)) by first creating normally distributed random numbers with standard deviation values according to the IASI level 1c noise values (*Peter Schluessel, EUMETSAT, private communications, 2000*) interpolated to the IASI wavenumbers. Since RTIASI

calculates apodized radiances and brightness temperatures this noise is convoluted with the instrumental spectral response function (ISRF) of the IASI instrument which is a 0.5 cm^{-1} full width at half maximum (FWHM) Gaussian with a cardinal sinc function (*Cayla* (1996)). Additionally, the noise is properly scaled, based on the Planck law, from the reference temperature of the IASI level 1c noise values to the actual brightness temperatures calculated by RTIASI (details in section 2.4).

2.2 Retrieval Algorithm

Since real measurements will be noisy, which means that they are subject to experimental errors, the retrieval algorithm has to account for these measurement uncertainties. A helpful and general way of dealing with noisy inverse problems is the *Bayesian* approach (for a detailed description of this problem see, e. g., *Rodgers* (2000)), where *a priori* knowledge (or expectation) of a state quantity is combined with new measurement information. In particular, *Bayes' theorem* tells, how an imperfect measurement (resulting from experimental errors), quantified by a probability density function (pdf) maps into the state space and is combined there with an as well imperfect prior knowledge of the state, which is quantified by a pdf, too.

Since our optimal estimation problem is moderately nonlinear, we utilize the iterative Gauss-Newton optimal estimation algorithm (c.f. *Rodgers* (2000)):

$$\mathbf{x}_{i+1} = \mathbf{x}_{ap} + \mathbf{S}_i \, \mathbf{K}_i^T \mathbf{S}_\epsilon^{-1} \left[(\mathbf{y} - \mathbf{y}_i) - \mathbf{K}_i \left(\mathbf{x}_{ap} - \mathbf{x}_i \right) \right], \tag{3}$$

where i is the iteration index, $\mathbf{x}_{ap}$ is the *a priori* profile (combined state vector consisting of a temperature, humidity, and ozone profile, and an SST value), $\mathbf{S}_i$ is the retrieval error covariance matrix,

$$\mathbf{S}_i = \left(\mathbf{K}_i^T \mathbf{S}_\epsilon^{-1} \mathbf{K}_i + \mathbf{S}_{ap}^{-1} \right)^{-1}, \tag{4}$$

$\mathbf{K}_i$ is the Jacobian Matrix evaluated at $\mathbf{x} = \mathbf{x}_i$, $\mathbf{S}_\epsilon$ is the measurement error covariance matrix, and $\mathbf{y}_i = \mathbf{f}(\mathbf{x}_i)$ is the measurement estimate for state $\mathbf{x}_i$.

Applying Eq. 3 we initialized the iteration with $\mathbf{x}_i = \mathbf{x}_{ap}$ and updated the state estimate $\mathbf{x}_i$, the measurement estimate $\mathbf{y}_i$, the estimate of the Jacobian matrix $\mathbf{K}_i$, and the estimate of the retrieval error covariance matrix $\mathbf{S}_i$ at each iteration step.

The convergence criterion for Eq. 3 is given by (c. f. *Rodgers* (2000)):

$$\chi^2 \leq m, \tag{5}$$

where m is the number of used measurement channels and the cost function χ^2 is given by:

$$\chi^2 = (\mathbf{y} - \mathbf{y}_i)^T \, \mathbf{S}_\epsilon^{-1} \, (\mathbf{y} - \mathbf{y}_i) + (\mathbf{x}_i - \mathbf{x}_{ap})^T \, \mathbf{S}_{ap}^{-1} \, (\mathbf{x}_i - \mathbf{x}_{ap}) \, . \tag{6}$$

If this criterion is not met, the iteration loop is terminated either if $\chi_i^2 \geq \chi_{i-1}^2$ (i. e., if χ^2 starts to increase again) or if the number of iterations, i, exceeds 6, respectively. Due to linearization errors the first or the first two iterations may need special aid with convergence acceleration which we solved by applying the so called *D-rad* method (*Liu et al.* (2000); *Lerner et al.* (2002)).

2.3 Error Characterization Functions

For a detailed investigation of retrieval result from use of Eqs. 3 and 4, a characterization is needed which provides useful insight into the properties of the retrieved profiles (e. g., *Rodgers* (2000); *Rieder and Kirchengast* (2001)). Hence, we are examining the gain matrix (or contribution matrix), $\mathbf{G}$, which expresses the sensitivity of the retrieved state, $\hat{\mathbf{x}}$ (the finally accepted best state estimate), to the measurement $\mathbf{y}$, $\mathbf{G} = \partial\hat{\mathbf{x}}/\partial\mathbf{y} = \hat{\mathbf{S}}\hat{\mathbf{K}}\mathbf{S}_\epsilon^{-1}$, where $\hat{\mathbf{S}}$ is the retrieval

error covariance matrix of the best estimate and $\hat{\mathbf{K}}$ is the final estimate of the linearized forward model. The columns of $\mathbf{G}$, the gain or contribution functions, quantify how much a specific measurement $\mathbf{y}(m)$ (with m as the channel number) contributes to $\hat{\mathbf{x}}$.

Additionally, the averaging kernel matrix, $\mathbf{A}$, and the signal-to-noise ratio matrix, $\tilde{\mathbf{K}}$, are of interest. $\mathbf{A}$ is defined by $\mathbf{A} = \partial\hat{\mathbf{x}}/\partial\mathbf{x} = \mathbf{G}\hat{\mathbf{K}}$ and denotes the sensitivity of the retrieved state, $\hat{\mathbf{x}}$, to the "true" state, $\mathbf{x}$. The rows of $\mathbf{A}$, the averaging kernel functions, also termed resolution kernels, generally peak at the diagonal of $\mathbf{A}$, and the width at half maximum of this peak is a rough measure of the vertical resolution of $\hat{\mathbf{x}}$ at the height level of the peak. An alternative measure of the vertical resolution was introduced by Backus and Gilbert 1970 (c. f. *Rodgers* (2000)). The Backus-Gilbert measure defines the resolution r_i at a height level i, with Δz_j as the height interval at level j (half level above minus half level below) as follows,

$$r_i \equiv 12 \, \frac{\sum_j (z_i - z_j)^2 \, \frac{A_{ij}^2}{\Delta z_j}}{\left(\sum_j A_{ij}\right)^2}, \tag{7}$$

In the case of negative sidelobes in $\mathbf{A}$ we may substitute A_{ij} by $|A_{ij}|$ in the denominator, otherwise the calculated resolution would be too large (*Collard* (1998)).

Given the definitions of the gain matrix and the averaging kernel matrix it is instructive to decompose the retrieval error covariance matrix $\hat{\mathbf{S}}$ into two components of the form,

$$\hat{\mathbf{S}} = (\mathbf{A} - \mathbf{I}_n)\, \mathbf{S}_{ap}\, (\mathbf{A} - \mathbf{I}_n)^T + \mathbf{G}\mathbf{S}_\epsilon\mathbf{G}^T, \tag{8}$$

with $\mathbf{I}_n$ as the identity matrix of dimension n. The first term on the right-hand-side is the so called smoothing error covariance matrix which expresses the contribution of the *a priori* error to $\hat{\mathbf{S}}$. The second one is the measurement-based error covariance matrix representing the contribution of the measurement errors.

The last characterization function utilized is the signal-to-noise ratio (SNR) given by the SNR matrix defined by $\tilde{\mathbf{K}} \equiv \mathbf{S}_\epsilon^{-\frac{1}{2}}\hat{\mathbf{K}}\mathbf{S}_{ap}^{\frac{1}{2}}$, where the diagonal elements of $\tilde{\mathbf{K}}$ estimate the SNR profile associated with $\hat{\mathbf{x}}$ and its rows, the so-called SNR functions, indicate the relative influence of measurement and *a priori* uncertainties at different height levels, respectively. More thoroughly exploited, the number of singular values of $\tilde{\mathbf{K}}$ greater than about unity expresses the effective number of independent measurements made to be better than the measurement noise level.

2.4 Covariance Matrices

For the current study the *a priori* error covariance matrix was obtained by first calculating the root mean square (rms) profiles of temperature and humidity for a set of more than 500 000 profiles between an ECMWF analysis field and its corresponding 24-h forecast field at the geographic locations of the ECMWF horizontal grid but interpolating the height grid to the RTIASI pressure level grid. To minimize perturbation effects of the obtained covariances on the retrieval, the rms was afterwards approximated by straight lines, selecting conservative outer bounds to the estimated rms profiles.

For the standard deviation values for the 2m temperature and the surface skin temperature the values of the last valid RTIASI pressure level have been kept constant. The standard deviation values for ozone have been set to 20% over the whole treated atmosphere. These fixed values for the standard deviations are summarized in Table 2. The values at all RTIASI pressure levels are obtained via linear interpolation between these prescribed values at fixed levels.

Since the RTIASI pressure levels define a quite dense grid, especially in the lower atmosphere, correlations between the levels have to be taken into account. We assume non-diagonal elements of the different *a priori* error covariance matrices with correlation lengths $L = 6$ km for

Temperature				
Pressure [hPa]	0.10	1.50	10.00	1013.25
StDev [K]	4.00	4.00	1.50	1.50
Humidity				
Pressure [hPa]	100.00	200.00	400.00	1013.25
StDev [%]	10.00	60.00	60.00	20.00
Ozone				
Pressure [hPa]	0.10	100.00	300.00	1013.25
StDev [%]	3.00	3.00	10.00	10.00

Table 2: Standard deviation (StDev) values at "anchor" pressure levels (Pressure) for temperature, humidity, and ozone for the simulation setup. The vertical transition between different StDev values was modeled linearly.

temperature, $L = 3$ km for humidity, and $L = 10$ km for ozone obeying an exponential drop-off according to,

$$S_{ij} = \sigma_i \sigma_j \exp\left[\frac{|z_i - z_j|}{L}\right], \tag{9}$$

where $\sigma_i = \sqrt{S_{ii}}$ is the standard deviation at level i and $z_{i,j}$ denote the height in kilometers at the particular pressure levels i and j, respectively. The height, z, was calculated for this purpose by utilizing the hydrostatic equation $z = -H \log(p/p_0)$, with a scale height, $H = 7$ km, and a surface pressure, $p_0 = 1013.25$ hPa.

In order to create an appropriate and consistent measurement error covariance matrix, $\mathbf{S}_\epsilon$, we assume the squares of the IASI standard noise values (level 1c noise values) to be the diagonal elements – properly adapted to the actual brightness temperature and reflecting forward model deficiencies by adding 0.2 K for all channels (c. f. *Collard* (1998); *Lerner et al.* (2002)). Additionally, non-diagonal elements were adopted, assuming an inter-channel correlation up to the third neighboring channel to account for the apodization process involved in the spectrum (see *Lerner et al.* (2002) for more detail). This produces a covariance matrix with a rather steep descent from the main diagonal.

Dependent on the quality of the *a priori* profile, the first or the first two iteration steps may need special aid with convergence due to linearization errors. Therefore $\mathbf{S}_\epsilon$ is modified in its diagonal according to (*Liu et al.* (2000)),

$$\mathbf{S}_\epsilon(k,k) = \max\left[\frac{(\mathbf{y}(k) - \mathbf{y}_i(k))^2}{\alpha}, \sigma^2(k)\right], \tag{10}$$

where k is the channel index, i is the iteration index, σ^2 is the measurement noise variance, i. e., the original diagonal element of $\mathbf{S}_\epsilon$, and α is a control parameter which is set to 4 in this report following *Weisz et al.* (2003).

2.5 Channel Selection

Since the full IASI spectra contain 8461 channels it is essential to reduce this number and remove redundant information for performance and computational reasons. Hence, our task is to find an optimal subset of channels, which is sufficiently sensitive to the retrieved variables. For this purpose we follow the approach of *Lerner et al.* (2002) and *Weisz et al.* (2003). We first perform a raw elimination of regions of the IASI spectrum starting with those channels at wavenumbers larger than 2500 cm^{-1}. The reason for this is that according to the standard IASI Level 1c noise

values these channels have larger measurement errors compared to the remaining spectrum and that solar radiation contributions become relevant in this spectral range ($<4\mu$m).

For temperature, humidity and ozone profile as well as surface temperature sounding and with the luxury of high spectral resolution we can also exclude those channels – 1220-1370 cm^{-1} (N_2O, CH_4, and SO_2) and 2085-2220 cm^{-1} (CO and N_2O) – whose "foreign" gas emissions contribute significantly to the measured brightness temperatures. In section 3 we perform some specific single-parameter retrievals in order to evaluate them against the results of the joint retrieval. For those cases the spectral regions were further confined. For the temperature and humidity only retrieval, respectively, the channels ranging from 825-1100 cm^{-1} were excluded since there the "atmospheric window" as well as an ozone band is situated which are not needed in the case of temperature and humidity profiling. On the other hand, the "atmospheric window" channels, more precisely, those channels between 825 cm^{-1} and 975 cm^{-1}, were used to perform the SST-only retrieval.

After this raw elimination of spectral regions we have about 6200 channels (for the full joint retrieval) which is still far too much for most operational and climatological applications as well as from the point of view of efficient numerical analysis and performance (e. g., *Press et al.* (1992)). It was instructively shown in *Rodgers* (1996) that it is no advantage to utilize all pieces of information, since they are highly redundant for most purposes. Thus we perform a further reduction of the number of channels by utilizing two different methods: the information content (IC) approach and the maximum sensitivity (MS) approach, respectively.

2.5.1 Information Content Theory

"Information" is a very general term that has been quantified in different ways by different authors. The measure for information content we refer to here is based on the information theory developed by Shannon in the 1940's (c. f. *Shannon and Weaver* (1976)).

The information content, H, of one measurement can be viewed as the information about a state gained by including a measurement, or alternatively, as the corresponding reduction in uncertainty. H defined from this point of view is a scalar measure and can be expressed as the logarithm to base two of the ratio of the prior to the posterior error covariance matrices (c. f. *Rodgers* (1996)),

$$H = \frac{1}{2} \log_2 \left| \mathbf{S}_{ap} \mathbf{S}^{-1} \right|, \tag{11}$$

where $\mathbf{S}_{ap}$ is the *a priori* error covariance matrix and $\mathbf{S}$ is the retrieval error covariance matrix defined by Eq. 4. If we now select the channels sequentially by retaining the channel with highest H and removing it afterwards from the subsequent calculations we obtain:

$$H_i = \frac{1}{2} \log_2 \left| \hat{\mathbf{S}}_i^{-1} \hat{\mathbf{S}}_{i-1} \right|. \tag{12}$$

This selection method is implemented in the way that at first the total number of IASI channels is pre-sorted according to the pressure levels where the weighting functions of the channels are peaking. The information content is then calculated using Eq. 12 for every available channel at each specific pressure level, starting with $\mathbf{S}_0 = \mathbf{S}_{ap}$. The number of selected channel per level is determined by taking 10% of the total number of peaking channels. Additionally, maximum and minimum threshold numbers of channels are defined following *Lerner et al.* (2002), for which the values used in this report are summarized in Tables 3 and 4.

These maximum and minimum thresholds are varying according to the average number of selected channels and to the retrieval scheme (for temperature there are two sets defined according to the pressure level range of the humidity retrieval, i. e., upper set: level 1-16; lower

set: level 17-43). The explicit number of channels, n, was computed as follows (c. f. *Lerner et al.* (2002)),

$$n = \min\left\{\min\left[n_{peak}, \max\left(\text{nint}(f \cdot n_{peak}), n_{min}\right)\right], n_{max}\right\}, \tag{13}$$

where n_{peak} is the number of weighting functions peaking at the currently treated level, f is the fractional factor which was set 0.1 (10%) in this report, and n_{min} and n_{max} are the minimum and maximum threshold numbers defined in Tables 3 and 4.

Joint Temperature, Humidity, Ozone, SST						
Temperature						
	levels < 100 hPa			levels > 100 hPa		
	min	medium	max	min	medium	max
n_{min}	1	5	10	2	9	13
n_{max}	2	9	13	3	13	23
Humidity						
	levels < 100 hPa			levels > 100 hPa		
	min	medium	max	min	medium	max
n_{min}	0	0	0	2	10	17
n_{max}	0	0	0	4	18	35
Ozone						
	levels < 100 hPa			levels > 100 hPa		
	min	medium	max	min	medium	max
n_{min}	5	20	30	5	20	30
n_{max}	6	30	50	6	30	50
SST						
	levels < 100 hPa			levels > 100 hPa		
	min	medium	max	min	medium	max
n_{min}	0	0	0	60	60	60
n_{max}	0	0	0	80	80	80

Table 3: Minimum and maximum threshold numbers for the determination of selected channels for multi-parameter retrieval.

2.5.2 Maximum Sensitivity Approach

As an alternative which is simpler than the IC approach above, an approach solely based on the weighting function matrix scaled by the measurement errors is evaluated (c. f. *Weisz et al.* (2003)). The method tries to selectively choose those channels whose instrument noise is small or the measurement sensitivity to the treated atmospheric constituent (temperature, humidity, ozone, or sea surface temperature) is high. This is accomplished by maximizing sensitivity-to-error ratios, gathered in a matrix defined as,

$$\mathbf{H} = \mathbf{S}_{\epsilon}^{-\frac{1}{2}}\mathbf{K}, \tag{14}$$

where the measurement error covariance matrix, $\mathbf{S}_{\epsilon}$, is taken as a diagonal matrix by ignoring the inter-channel correlation for this purpose. The square-root of the inverse of $\mathbf{S}_{\epsilon}$, more precisely, the inverse square-roots of its diagonal elements (the standard deviations) are expressing the uncertainty of a measurement, i. e., $\mathbf{S}_{\epsilon}$ is used to sensibly weigh in the quality of the measurement.

Single Temperature Retrieval						
	levels < 100 hPa			levels > 100 hPa		
	min	medium	max	min	medium	max
n_{min}	1	20	70	2	25	75
n_{max}	2	25	90	3	35	90
Single Humidity Retrieval						
	levels < 100 hPa			levels > 100 hPa		
	min	medium	max	min	medium	max
n_{min}	0	0	0	2	30	80
n_{max}	0	0	0	4	50	95
Single SST Retrieval						
	levels < 100 hPa			levels > 100 hPa		
	min	medium	max	min	medium	max
n_{min}	0	0	0	60	60	60
n_{max}	0	0	0	80	80	80

Table 4: Minimum and maximum threshold numbers for the determination of selected channels for single-parameter retrieval.

Advancing further the approach of *Weisz et al.* (2003), the implementation of this channel selection algorithm starts once more with using the pre-information where the weighting functions of the channels are peaking (c. f. section 2.5.1). Then the sensitivity-to-error ratio matrix is calculated one time and a specific number of channels is selected per level in the same way as in the IC approach. The usage of the pre-information where the weighting functions of the channels are peaking yields systematically better retrieval performance results in the subsequent estimation process than applying the IC or MS approach just globally to the channels.

For illustrating the relevance and performance of adequate channel selection, Figure 1 shows two different numbers of selected channels (310, panels a,c and 909, panels b,d) for the two channel selection methods (IC approach, panels a,b, and MS approach panels c,d). The dashed-dotted and dotted vertical lines are delimiting the specific spectral regions for the selection of surface skin temperature channels (825 cm^{-1} – 975 cm^{-1}) and ozone channels (650 cm^{-1} – 750 cm^{-1} and 975 cm^{-1} – 1100 cm^{-1}), respectively. The four spectral regions for selecting the temperature and humidity channels are delimited by the vertical solid black lines (645 cm^{-1} – 825 cm^{-1}, 1100 cm^{-1} – 1220 cm^{-1}, 1370 cm^{-1} – 2085 cm^{-1}, 2220 cm^{-1} – 2500 cm^{-1}).

The two selection methods show a quite similar behavior for the ozone channels (indicated by the crosses) whereas this is not the case for the surface channels (plus signs). A comparison of the two selection methods regarding the temperature profile channels (diamond symbols) exhibits similarities but also quite significant differences in the spectral region where they occur as well as in their distribution, especially in the case of selecting about 900 channels.

Inspecting panel b and panel d in detail we can see that in the case of the selection with the MS approach the channels are more accumulated in special spectral regions (near 700 cm^{-1}, between 1400 cm^{-1} and 1600 cm^{-1}, and around 2000 cm^{-1}). Additionally, the MS approach selects almost no channels at the ascending wing of the CO_2 band centered at 667 cm^{-1} which is done when using the IC approach. These differences are resulting in discrepancies especially in temperature-only retrievals (c. f., *Weisz et al.* (2003)).

Since the H_2O absorption covers the complete IASI spectral range (e. g., the ν_2 fundamental vibration mode ranging from 640 cm^{-1} to 2800 cm^{-1} and centered at 1600 cm^{-1}, or the H_2O continuum ranging from ∼200 cm^{-1} to 1200 cm^{-1}) there is no special spectral domain preferred

for the selection of channels in the allowed region. This behavior is illustrated well in all four panels of Figure 1.

Nevertheless the two methods show differences in the region where the H_2O channels are selected. The IC approach exhibits an accumulation of chosen channels between 1400 cm^{-1} and 1600 cm^{-1} and around 2000 cm^{-1} (c. f. the accumulation of the temperature channels selected with the MS approach) whereas the MS method has clusters of chosen channels near 2300 cm^{-1}.

It is to be learned and stressed in summary that an as intelligent as possible channel selection procedure is essential for a numerically efficient yet high-quality retrieval. Especially a clustering (accumulation of channels selected from the same spectral region and peaking at the same height region) of channels by a selection method which is too strong or ignoring crucial spectral regions, yields a marked degradation of the results. In the results section below we thus carefully assess the retrieval performances based on both the IC and MS approach for different total channel numbers used.

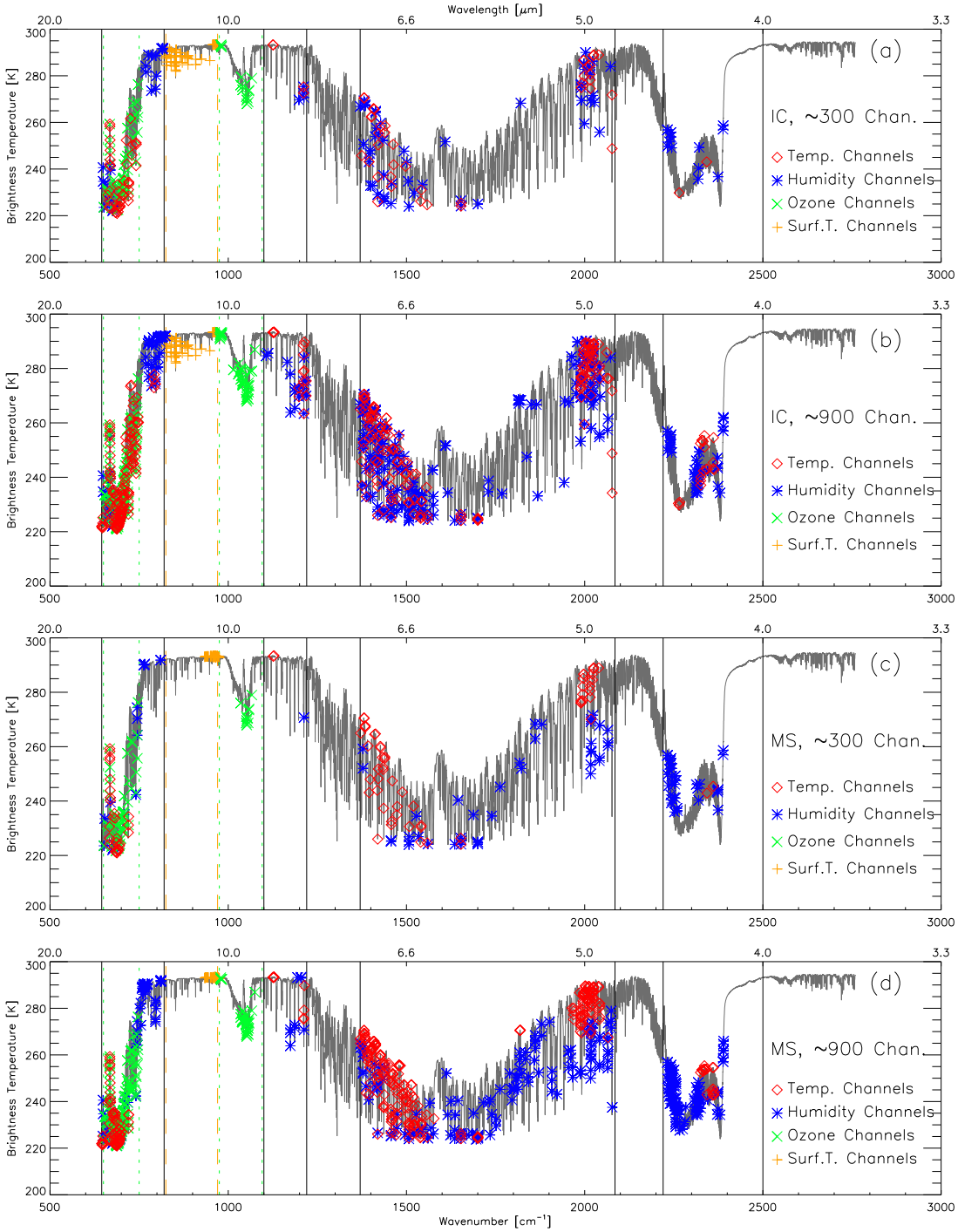

Figure 1: Selected channels for temperature, humidity, and ozone profiles as well as for SST overplotted on the brightness temperature spectrum calculated with RTIASI for a U. S. standard mid-latitude summer atmosphere. The diamonds indicate the temperature channels, the asterisks the humidity channels, the crosses the ozone channels and the plus signs the SST channels. Panels a and b depict the selection based on the IC approach whereas panels c and d the one for the MS approach. The total number of selected channels for panels a and c (adding the channels for all constituents) was 310, whereas the total number for panels b and d was 909. The vertical lines delimit the regions within which the channels for the different atmospheric species were selected. Solid lines: temperature and humidity, dashed lines: SST, dotted lines: ozone.

3 Performance Simulation Results and Discussion

3.1 Simulation Setup

The retrieval performance assessments discussed in this report were based on simulated data for a quasi-realistic orbit arc of MetOp with a full swath of the IASI instrument (for details on IASI sampling see e. g., http://smsc.cnes.fr/IASI/). The swath was modeled by first calculating the ground points of a MetOp sub-orbital track using a standard orbit software extracted from the Mission Analysis Planning System of the EGOPS (End-to-end GNSS Occultation Performance Simulator) software package (*Kirchengast et al.* (2002)) and then calculating the locations along sounding rays defined by the RTIASI pressure level grid via the principles of spherical trigonometry.

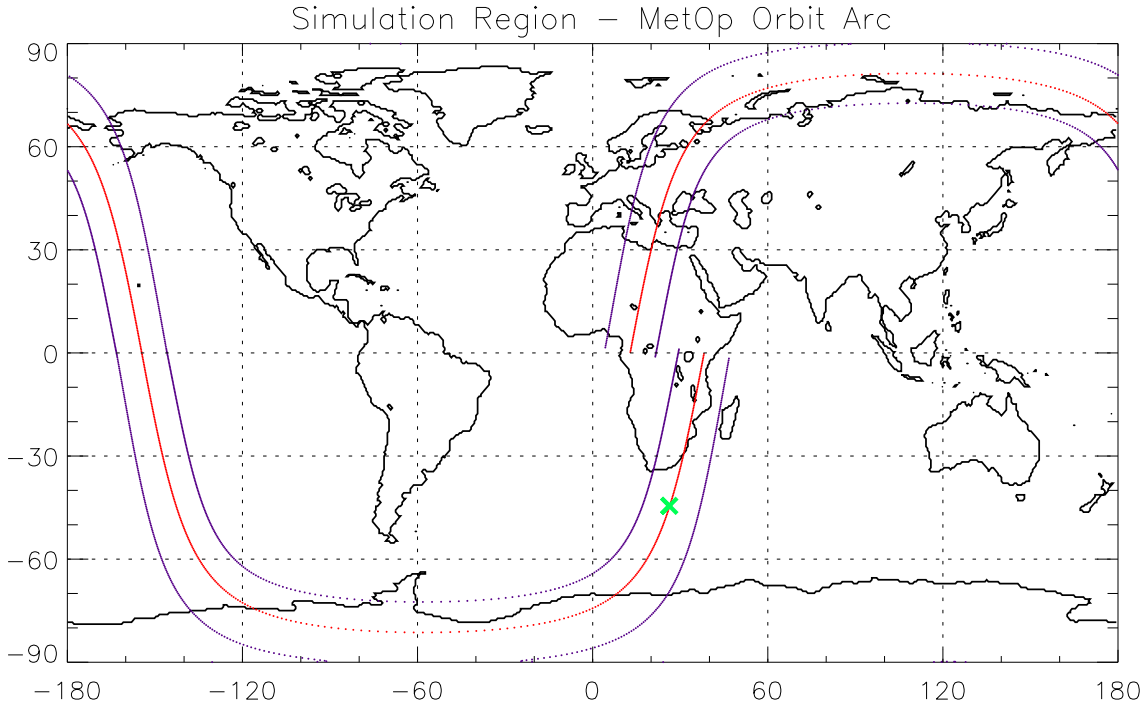

Figure 2: Ground track and lateral width of the IASI swath simulated for one MetOp orbit, depicted on a world map. The line of dots in the middle indicates the nadir points of the MetOp satellite for every 8-*th* second (IASI swath sampling time). The black cross is the position of the profile for which the error characterization functions are discussed.

The number of profiles for the full orbit resulting from this procedure is ∼22 800. Additionally, there are 15 233 surface pixels of sea surface temperature (surface skin temperature) data – the surface data shown here contain only the points over the ocean surface. Figure 2 shows the ground track and swath width of the simulation region – it is an orbit ranging from Africa over Antarctica, the Pacific Ocean and the Arctic region back to Africa via eastern Europe. The line of dots in the middle indicates the nadir points of the MetOp satellite for every 8-*th* second, the swath duration of IASI. The black cross indicates the location of the representative profile for which the error characterization functions are shown and discussed (section 3.3).

To obtain quasi-realistic atmospheric conditions a high resolution ECMWF analysis field (T511L60 resolution, e. g., *ECMWF* (2004)) from September 15, 2002, 12 UTC (date arbitrary selected), was used to create the "true" profiles. The individual values along the profiles were obtained by interpolating the values of the analysis field to the locations according the RTIASI pressure level grid. The version of RTIASI used in the current stage of the report is RTIASI 1.0

(*Matricardi and Saunders* (1999)). The forward model RTIASI (section 2.1) was used to simulate the IASI measurement spectra based on these atmospheric fields. To obtain quasi-realistic IASI spectra we added an additional Gaussian noise term, $\boldsymbol{\epsilon}$, according to the formulation of $\mathbf{S}_\epsilon$ given in section 2.4.

Temperature and Ozone were retrieved over the whole RTIASI pressure level range. Additionally, the surface air temperature (2 m temperature) and the surface skin temperature were added to the retrieval process to obtain an excellent surface retrieval. In the case of humidity only the lowest 28 levels (up to ∼100 hPa) were introduced in the joint retrieval since the stratosphere (at <100 hPa) is a very dry region and the humidity information which can be gained there by the IASI instrument is negligible.

For the initialization of and as *a priori* data to the retrieval we used the 24-hour ECMWF forecast field of the ECMWF analysis field (i. e., the 1-day forecast field for September 15, 2002, 12 UTC) for temperature and humidity. The *a priori* data for ozone and SST, where the 24 hour forecast is of no suitable help, were rather obtained by creating them consistent with the assumed *a priori* error covariance matrices (section 2.4) via the "error patterns method" described in detail in *Rodgers* (2000).

3.2 Performance Analysis of the Joint Algorithm

The aim of this section is to show the performance of the joint algorithm on the one hand and on the other hand to check the hypothesis that the quality of the retrieval does not decrease when using a climatology, more precisely the CIRA86aQ climatology (*Kirchengast et al.* (1999)) complemented by suitable ozone profiles obtained from U. S. standard profiles, for the channel selection process (section 2.5) instead of the short-term forecast profiles requiring repeated channel selection for each single sounding ray.

Figure 3 shows the results of the retrieval process for temperature (left column), humidity (middle column) and ozone (right column), respectively, for all ∼22800 profiles of the MetOp orbit arc. With the ECMWF profiles as "true" profiles, the panels show bias (solid black line), standard deviation (solid gray line), rms error (dashed black line), standard error (square-root of diagonal elements) specified in the *a priori* error covariance matrices (dashed-dotted black line), and, in panels d – i, standard error (square-root of diagonal elements) as defined in the retrieval error covariance matrices (dashed-dotted gray line), respectively. Panels a – c directly exhibit the errors of the *a priori* profiles compared to the "true" profiles showing that these have been conservatively set for temperature and humidity (outer-bound envelope to the error estimates for the present forecast-minus-analysis data used). Since ozone *a priori* data are produced consistent with the ozone *a priori* error covariance matrix these data of course exhibit an estimate error structure (standard deviation, rms error) identical with the standard error in the covariance matrix. Panels d – f exhibit the estimation results for the case when using the climatologies for the channel selection process, and panels g – i for the case when using the 24h-forecast data, respectively.

Comparing the temperature retrievals for both channel selection data sets, the one using the CIRA86aQ climatology (panel d) and the other using the 24h-forecast profiles (panel g), with the *a priori* data (panel a) we find that the bias arising in the stratosphere of <10 hPa could mostly be eliminated by the inclusion of the IASI measurement information. Furthermore, a decrease in standard deviation and rms, respectively, could be evidently gained, both in the stratosphere and the troposphere, where at levels >200 hPa the rms error was reduced to ∼0.5 K.

An overall comparison of the retrieval results for the two different channel selection data sets for all three atmospheric parameters (panels d – f vs. panels g – i) reveals that the differences are negligible. Since the usage of the climatology in the channel selection process is much more efficient than using the forecast data since in the former case the channels are selected into

latitude/month-dependent "lookup tables" only once while in the latter case the selection is part of every new profile retrieval, this is a very favorable result. Our future baseline for large-scale climatological application of the algorithm is thus to just use pre-selected channel sets in form of "lookup tables" which we have prepared in 5 degree latitude steps for each month of the year.

Comparing the results of the retrieved humidity with the first guess (panel b), mostly the same can be said as in the case of the estimation of temperature. We recognize that the standard deviation and rms error are systematically improved over the *a priori* error, with the retrieved humidity profile exhibiting an rms error of 15–20% throughout (<15% below 850 hPa). The small humidity biases, up to 3%, arise from non-linearities in the humidity retrieval caused by the relatively large *a priori* error.

In the case of the retrieved ozone profiles (panel f and i), we get moderate improvements of the ozone retrieval over the *a priori* data (panel c) proportional to the ozone concentration (i. e., best around the peak of the ozone layer). This is due to the fact that the weighting functions of ozone exhibit important peaks only at these heights (section 3.3). We also note that the performance of the ozone retrieval is rather independent from the *a priori* data and other described settings used for temperature and humidity which is also true vice versa.

Figure 4 illustrates the retrieval performance of the SST where again there is no visible difference between using CIRA86aQ (panel a) or the *a priori* data (panel b) in the channel selection process. The SST results show that the retrieval exhibits better results for the rms error than the theoretical estimate in the retrieval error covariance matrix (S_ret) proposes. This can be explained by the fact that the retrieval performance of SST is significantly aided by the retrieval quality of the overlying atmosphere (see also section 3.5 below), a dependence not fully reflected by the theoretical estimate.

Quantitatively, the SST retrieval is found very accurate at the ∼0.1 K level. The reason for this good performance, observed all over the swath, is the assumption of a clear sky all over the retrieval region. In the case of the presence of clouds the retrieval would in general stop at the cloud top and no SST sensitivity would exist. However, as cloudiness can be reasonable well detected (e. g., *Lavanant and Lee* (2005)) and as SST variability is small over a few days time scale, the results confirm that IASI is clearly a promising instrument for accurate SST sounding in an operational manner.

3.3 Profile Retrieval Characterization Results

In this section, basic error properties and characterization functions of the retrieval for a case of representative profiles of temperature and humidity are shown. The sounding location of this profile (44.5° south, 26.3° east) is illustrated in Figure 2. The profiles were chosen from the case of using climatology-based channel selection, for selecting ∼300 channels via the IC approach. In addition to the basic *a priori* and retrieval error characteristics we show characteristic properties of the retrieved temperature and humidity profiles including correlation functions, weighting functions, resolution kernels, gain functions, and signal-to-noise functions (section 2.3). This careful inspection of error/resolution/characterization properties provides a close understanding of the retrieval process and the algorithm.

3.3.1 Temperature

Figure 5 illustrates the error/resolution/characterization properties for temperature. Panels a and b instructively show that temperatures near the tropopause and in some stratospheric regions are most difficult to retrieve. The differences near the mid-latitude tropopause (∼200 hPa,

c. f. panel a) originate mainly from the limited vertical resolution of a nadir-looking sounder, even of an advanced one such as IASI.

Figure 5c illustrates various components of the estimated retrieval error of the temperature profiles. The estimated total errors (the square roots of the diagonal elements of $\hat{\mathbf{S}}$; Eq. 4) depend mainly on the shape of the weighting functions as well as on the assumed *a priori* errors. A closer examination shows that this total error estimate is mostly determined by the smoothing error (square roots of the diagonal elements of the smoothing error covariance matrix; Eq. 8) which is largest in the stratosphere where the *a priori* errors are important and the resolution kernels in $\mathbf{A}$ (section 2.3) are broad. The measurement-based error (the square roots of the diagonal elements of the measurement-based error covariance matrix; Eq. 8) depends on the shape of the gain functions in $\mathbf{G}$ (discussed below) and is comparatively small since the instrumental errors, specified in $\mathbf{S}_\epsilon$, are small.

Figure 5d gives a good indication of the influence of the *a priori* data on the retrieval by examining the "retrieval-to-*a priori*" error ratio profile (ratio of the estimated total retrieval errors to the *a priori* errors in percent). The 50% line (dotted vertical line) which is crossed by the ratio near 200 hPa implies that the *a priori* data have a major influence in the stratosphere, while the measurements improve more than a factor of 2 upon the *a priori* errors in the troposphere.

Panels e – i of Figure 5 illustrate further characteristics of this representative temperature profile, including error correlation functions of the *a priori* and measurement error covariance matrices (panel e), weighting functions (panel f), vertical resolution (panel g), gain functions (panel h), and SNR functions (panel i), respectively. The correlation functions (from rows of $\mathbf{S}_{ap}$ and $\hat{\mathbf{S}}$; Eq. 4 and section 2.4) are shown for clarity at three selected pressure levels only (∼400, ∼200, and ∼10 hPa), representing the troposphere, the tropopause region, and the stratosphere, respectively. Correspondingly, weighting functions (rows of $\mathbf{K}$), gain functions (columns of $\mathbf{G}$), and SNR functions (rows of $\tilde{\mathbf{K}}$; c. f. section 2.3) are shown for three representative channels only (1472.75, 694.25, and 649.0 cm^{-1}), which exhibit peaks at or close to the three pressure levels chosen above. The diamond symbols indicate the retrieval levels (i. e., represent the actual values of the matrices) illustrating the usage of a non-equidistant grid.

The correlation functions (rows of the normalized covariance matrix $C_{ij} = S_{ij}/\sqrt{S_{ii}S_{jj}}$) quantify the degree of correlation between the error at a given level i with one at any other level j. The correlation functions of the *a priori* error (solid lines in panel e) follow the exponential drop-off structure as specified in section 2.4. The retrieval errors obtained in $\hat{\mathbf{S}}$ show a somehow similar but significantly sharpened correlation structure (dashed lines in panel e). This indicates that the errors in the retrieved temperature profiles (but also those of the retrieved humidity profile, c. f. Figure 6 below) are much less correlated between neighboring levels. The sharpening is introduced into $\hat{\mathbf{S}}$ by the transformed-$\mathbf{S}_\epsilon^{-1}$ term dominating $\mathbf{S}_{ap}^{-1}$ in Eq. 4.

Figure 5f shows the characteristic shape of the weighting functions of temperature, where each function indicates the weighting with which the temperature profile contributes to the brightness temperature (T_B) observation of a particular IASI channel. While T_B observations sensitive to the troposphere (e. g., the 1472.75 cm^{-1} channel) stem from rather narrow well defined regions, the weighting functions increasingly broaden in the stratosphere, where their spread is of the order of 10 km (e. g., at 649.0 cm^{-1}). It is evident from this type of sensitivity (and based on the fact that more IASI channels peak in the troposphere than in the stratosphere) that the inversion will lead to retrievals with better resolution and accuracy in the troposphere than in the stratosphere.

Figure 5g illustrates the vertical resolution estimates of the retrieved temperature profile based on the Backus-Gilbert measure and the averaging kernel full-width at half maximum (FWHM) measure, respectively. The resolution is estimated 2-8 km in the troposphere (>200 hPa), and lower than ∼8 km upward into the stratosphere. This is coarser than other

estimates typical for IASI-retrieved temperatures (e. g., *Collard* (1998); *Weisz* (2001)), since we have employed a combination of a priori information with rather accurate *a priori* temperatures and rather relaxed accuracy of a priori humidity. This conservative specification does not emphasize good temperature resolution, though it is practically significantly better than formally estimated (c. f. panels 5a-b), but good humidity resolution (see Figure 6 below) and better independence of retrieved profiles from *a priori* data.

The gain functions (Figure 5h) indicate that any specific observation contributes most to the retrieved profile near the peak of the associated weighting function. At first view it may contradict intuition, given the better retrieval performance in the troposphere, that the smallest gain occurs for the tropospheric channel. But on a deeper view we note that the stronger gain function of the higher altitude channels does not only mean higher sensitivity of the retrieved state of the temperature to the measured brightness temperature of an individual channel but also a correspondingly higher error amplification. Thus, in contrast to the weighting functions, the gain functions do not directly indicate retrieval performance.

SNR functions (Figure 5i) resemble the shape of the weighting functions since they are just normalized versions of them (c. f. section 2.3). In the troposphere their magnitude is governed mainly by the small measurement errors whereas in the stratosphere they are dominated by the larger *a priori* errors.

3.3.2 Humidity

Figure 6 illustrates the error/resolution/characterization properties for humidity in the same way as Figure 5 above for temperature. Panels a and b show that the largest part of information can be gained in a region between 700 hPa and 200 hPa. Problems arise at heights lower than about 700 hPa due to less information gained by the IASI instrument in this region and comparatively smaller *a priori* errors in the lowest few kilometers above the surface. The particularly big difference between ∼900 and ∼750 hPa are evidently explained by the fact that the forecast (*a priori*) did not accurately catch the height of the maritime boundary layer (see panel a) and since this is a very sharp humidity gradient structure the resolution of the IASI instrument is as well too low to resolve it. This better performance especially in the ∼600 – 250 hPa height range is also indicated by panel c, showing an increase of measurement and smoothing errors below 600 hPa and above ∼250 hPa as well as by panel d, showing that the "retrieval-to-*a priori*" error ratio lies below 50% also just between ∼600 – 250 hPa. For our climatological interest in particular in upper troposphere water vapor this performance at <600 hPa is very encouraging.

The characterization functions (panels e – i) which were theoretically well explained in the temperature section above, are also shown here for three selected pressure levels (∼840 hPa, ∼360 hPa, and ∼220 hPa) where the first one represents the lower troposphere and the two other ones the upper troposphere, respectively. Corresponding channels, as displayed in case of the weighting functions, gain functions and SNR functions are selected at 852.25 cm^{-1}, 1472.75 cm^{-1}, and 1558.0 cm^{-1}, respectively.

Error correlation (Figure 6e) behaves quite analogously to temperature (Figure 5e). The weighting functions for humidity (Figure 6f) exhibit a reasonably narrow shape, which contributes to a good vertical resolution throughout the whole tropospheric region (Figure 6g). The Backus-Gilbert and Averaging Kernel FWHM measures estimate a vertical resolution of about 2 km in the lower and middle troposphere (>350 hPa), which gradually increases to about 3 km or more near 200 hPa, which is similar to other estimates (e. g., *Collard* (1998); *Camy-Peyret and Eyre* (1998)). The "bump" near 700 hPa, stronger in the Backus-Gilbert measure than in the FWHM measure, together with more emphasis on *a priori* information (panel 6d), indicates somewhat less weight of IASI data in this region. Inspecting a broader ensemble of globally distributed profiles in this way (not shown) indicates that this effect is limited to specific

atmospheric conditions only.

Gain and SNR functions (Figure 6h,i) appear to show similar characteristics as discussed for the tropospheric temperature case, and again indicate the favorable sensitivity of IASI especially for upper troposphere humidity sounding.

3.4 Performance Comparison of IC and MS Channel Selection

In this section the retrieval performance based on the two different channel selection algorithms described in section 2.5 (IC and MS approach) is comparatively assessed for three sets of numbers of selected channels. For all six cases we used the same orbit arc datasets as in section 3.2 above, whereby we chose here the climatology-based (CIRA86aQ and U. S. standard atmosphere ozone) channel selection. The assessment is to reveal which channel selection approach is to be potentially preferred and whether a channel reduction to as low as ∼300 channels is possible without relevant performance degredation of the joint algorithm retrieval products.

The three different sets of numbers of selected channels were chosen with the target to get approximately 3.5%, 10% and 20% of the full number of IASI channels (8461) which resulted in an averaged number of selected channels per profile of ∼300 (300) channels for the smallest dataset (∼3.5%), ∼900 (887) channels for the medium dataset (∼10.6%), and ∼1800 (1808) channels for the largest dataset (∼21.3%). On a closer examination this can be split up into the different atmospheric parameters (and SST) the channels are selected for. To this end, more precisely, the averaged numbers of selected channels per profile were 89/ 324/ 858 channels for temperature, 87/ 336/ 766 for humidity, 64/ 167/ 224 for ozone and 60/ 60/ 60 for SST, respectively. We see that the number of selected channels for the different atmospheric species do not follow the rough multiplication factors between total sets (3.5%×3 ≈10%; 10%×2 = 20%). The reason is that the IASI spectral interval has only two small bands for the surface (SST) and the ozone channels (c. f. Figure 1) which means that the number of channels with reasonable information for these parameters is limited. Thus we have filled up the remaining amount by temperature and humidity channels.

Numerical Efficiency		
channel set	**IC**	**MS**
300	1.00	0.98
887	3.74	4.25
1808	11.25	13.13

Table 5: Comparison of the numerical efficiency for the six different channel selection cases normalized to the set with 300 channels selected by the IC approach.

Figure 7 (for temperature) and Figure 8 (for humidity) illustrate the inter-comparison of the results for the different cases. Ozone and SST inter-comparison are not explicitly shown. As they do not add further aspects to the discussion and conclusions we draw from assessing temperature and humidity. An overall view on Figures 7a-f and 8a-f already provides clear evidence that the performance differences are fairly small amongst all 6 cases although the numerical efficiency is of course drastically better for the case of selecting about 3.5% of the channels only. Table 5 summarizes the numerical efficiency (needed CPU time) normalized to the IC/300 channels case. It is seen that in the case of the small number of selected channels, both retrievals (with IC and MS approach) have the same performance (apart from small differences) whereas with an increasing number of channels the cost in computer time increases more than linearly.

On a closer examination of the temperature results (Figure 7) we serve that the theoretical estimation of the retrieval error (err. S_ret) is decreasing slightly with increasing number of

selected channels. This is not the fact for the actual rms error, however, which is virtually the same for the ∼300 and ∼900 sets but increases markedly for the case of ∼1800 selected channels. Furthermore, the ∼1800 set leads to the appearance of slight bias structures which are smaller in the two other sets. The reason why the practical performance is not strictly following the theoretical expectation has already been well outlined by *Lerner et al.* (2002): while in theory we tacitly assume error-free numerical computations in practice numerical residual error effects offset the theoretical gain, and in our system start to exceed it at near 1000 channels.

A comparison of the two different channel selection approaches (Figure 7 left column IC; right column MS) exhibits no significant difference for ∼300 and ∼900 channel cases. Only the ∼1800 channel case shows a slightly better performance for the IC approach which can be traced back to the fact that the IC approach selects fewer linearly dependent channels, in the sense explained in section 2.5 above.

Inspecting the humidity results more closely (Figure 8), we find that these show analogous behavior to the temperature results, i. e., no explicit gain in retrieval performance but rather increasing numerical residual error effects for an increasing number of channels. On an adequate and sufficient number of channels for the joint algorithm we thus conclude that ∼300 channels is an excellent and numerically efficient choice; even lower numbers start to imply performance degradation.

Regarding the preferable channel selection approach, we find that the MS approach has fairly the same but no better efficiency as the IC approach and closely similar but no better performance. Tentatively the IC approach performs slightly better, presumably due to the more even distribution of the selected channels (c. f. section 2.5), and the IC approach has theoretically a better foundation, so that we chose this one as the baseline for future large-scale application of the algorithm.

3.5 Comparison to Single Parameter Retrievals

We evaluated for the joint retrieval algorithm developed in this study how it improves over more specific single-parameter retrieval setups. This provides valuable further tests on the robustness and quality of the joint algorithm, but also allows to assess to what degree more simplified (and thus even faster) setups may be applicable. As input set for all cases discussed here, we used climatology-based channel selection by the IC approach for selecting ∼300 channels in total and again the full orbit arc dataset.

Figure 9 illustrates the results comparing joint retrieval to single-parameter retrieval where single-parameter retrieval means that one parameter (e. g., temperature) is retrieved while the others (e. g., humidity, ozone, SST) are kept fixed at their *a priori* values. We do not separately discuss ozone here since its retrieval is rather independent of the other parameters (section 3.2), so that the results of joint and single-parameter retrieval are essentially the same.

Regarding temperature (Figure 9a, b) we can identify two regions, which were also noted in an earlier study based on a temperature-only retrieval (*Weisz et al.* (2003)), where a loss in retrieval quality is incurred due to temperature only retrieval. The first is the boundary layer where on the one hand a detailed analysis of the results yielded a warm bias in the tropical and mid-latitude region originating from a warmer surface than the overlying atmosphere and on the other hand a cold bias occurring over Antarctica where the surface is generally colder than the atmosphere. This problem is mainly resulting from the absence of a simultaneous SST retrieval based on the inclusion of surface channels, as done in the joint retrieval. The second region where the joint retrieval algorithm is clearly superior is the troposphere (below 200 hPa) where the absence of the simultaneously retrieved humidity results in rms temperature error increases of more than a factor of 2. For stratospheric retrievals the differences are small; still more bias vulnerability and somewhat increased rms error is visible in the lower stratosphere

(below 20 hPa), however.

Regarding humidity (9c,d) the essential difference is evidently that the joint retrieval can achieve an rms error of no more than ∼15% throughout the free troposphere (c. f. section 3.2) while humidity-only retrieval achieves ∼20% or less.

This is since the joint retrieval accounts for the temperature-humidity coupling, while the humidity-only retrieval cannot do so. Still the latter works fairly well here thanks to the high quality, unbiased *a priori* temperature profiles from the ECMWF 24h forecast; in the case of a worse temperature input, the humidity-only retrieval may also incur biases up to ∼10%.

Regarding SST (Figure 9e, f), the joint temperature, humidity, ozone, and SST retrieval shows a drastically improved performance with an rms error at the ∼0.1 K level, whereas the SST only retrieval exhibits a small bias and an rms error not much reduced from the *a priori* uncertainty (1.5 K) used as input.

Closer examination of the error analysis results show that the main reason for this large difference lies in the tropics, more exactly, in regions with warm sea surface temperature. The main physical reason behind is the significant water vapor continuum absorption over warm tropical oceans even in the "atmospheric window" channels (e. g., *Liou* (2002)) which strongly degrades the SST-only retrieval. Even tests where we used "true" temperature or "true" humidity profiles, respectively, while leading to a better performance did clearly fail to reach the quality obtained by the joint algorithm. Simultaneous estimation of the overlying atmosphere, as done in the joint algorithm, is thus essential for a high quality SST retrieval, in particular for the low latitude region.

In summary it is clear that the joint temperature, humidity, ozone, and SST retrieval algorithm exhibits a significantly improved performance over the single-parameter retrieval setups, and is thus our obvious baseline for future large-scale application. While this is itself neither new nor surprising the understandable and robust way in how our newly developed IASI processing system behaves both in joint and single-parameter mode provides us with substantial confidence in its utility for future applications.

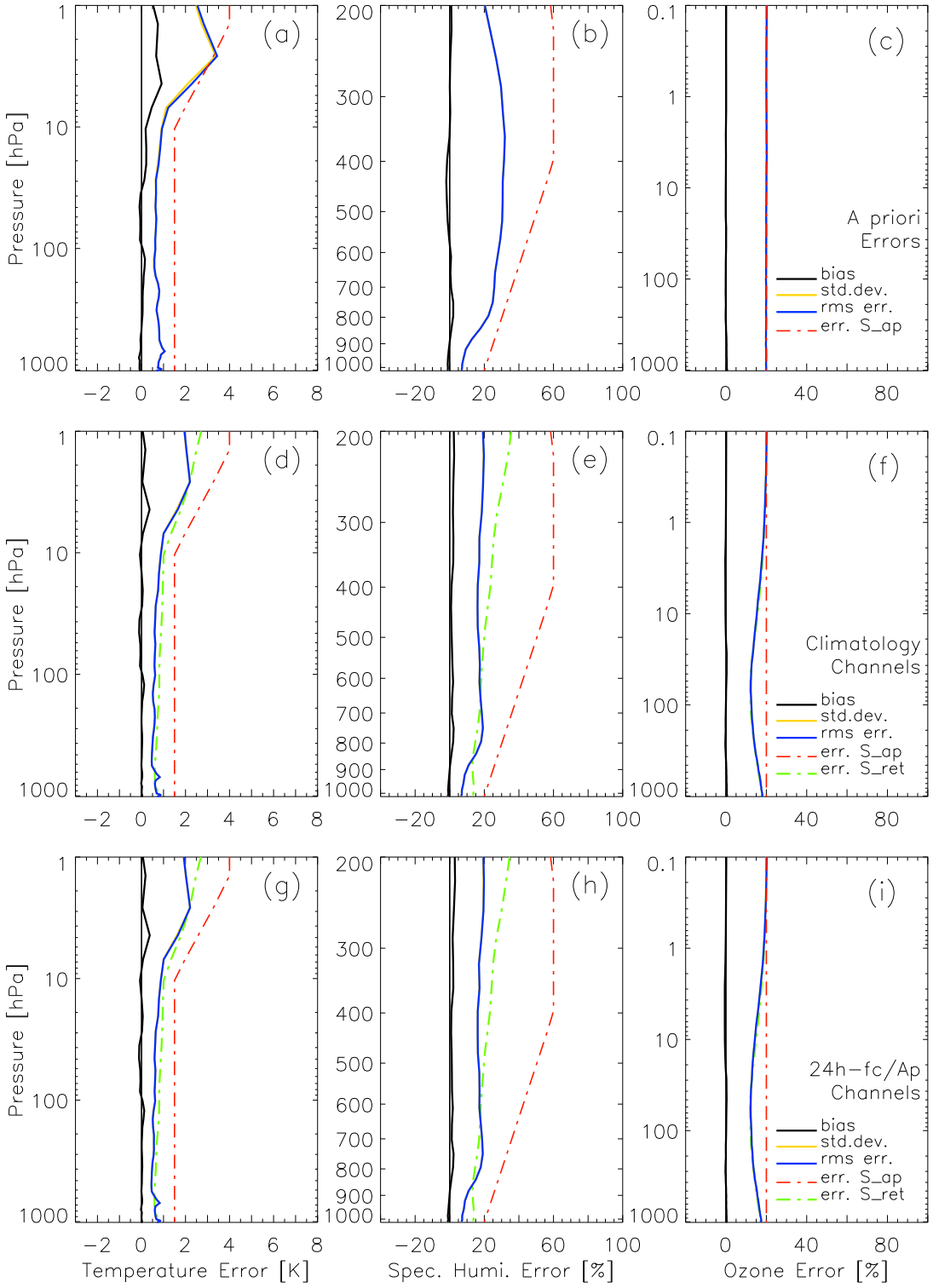

Figure 3: Results of the joint retrieval algorithm for temperature (left column), humidity (middle column) and ozone (right column). Bias (solid black line), standard deviation (solid gray line), rms error (dashed black line), standard error (square-root of diagonal elements) specified in the *a priori* error covariance matrices (dashed-dotted black line), and, in panels d – i, standard error (square-root of diagonal elements) as defined in the retrieval error covariance matrices (dashed-dotted gray line). Panels a – c direcly exhibit the errors of the *a priori* profiles compared to the "true" profiles.

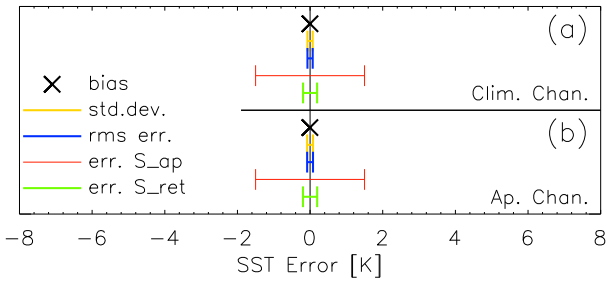

Figure 4: Results of the joint retrieval algorithm for SST. Bias (black cross), standard deviation (dark-gray error bars), rms error (black), standard error (square-root of diagonal element) specified in the *a priori* error covariance matrices (light black), and, standard error (square-root of diagonal element) as defined in the retrieval error covariance matrices (light gray).

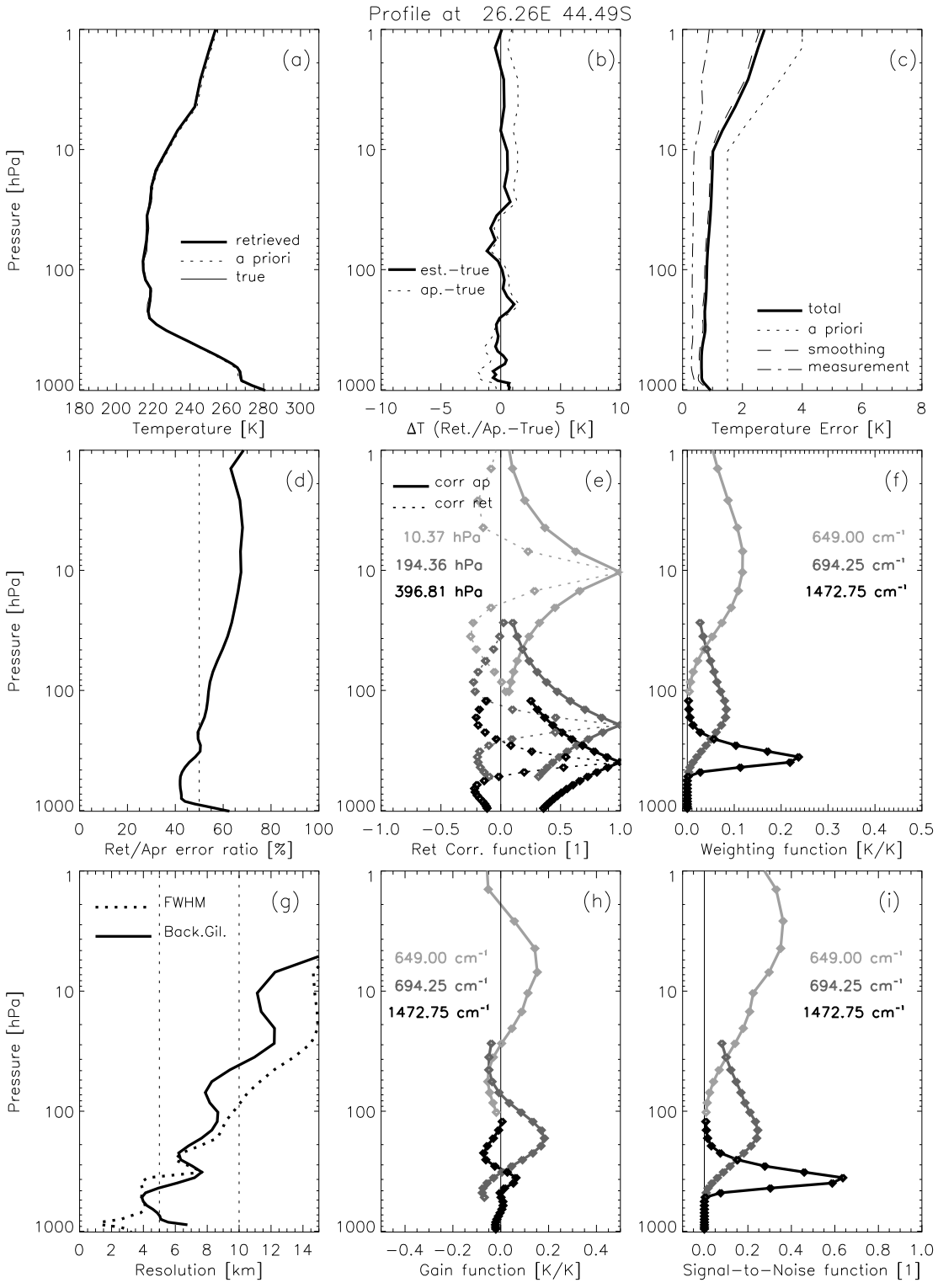

Figure 5: Optimal estimation results for the error analysis and various functions characterizing the retrieval performance (c. f. section 2.3) for a representative mid latitude temperature profile (44.5° S, 26.2° E; c. f. Figure 2). For clarity, the characterization functions are shown for three representative levels (∼400, ∼200, and ∼10 hPa) and channels (1472.75, 694.25, and 649.0 cm^{-1}) only. See text for explanation and discussion of the panels.

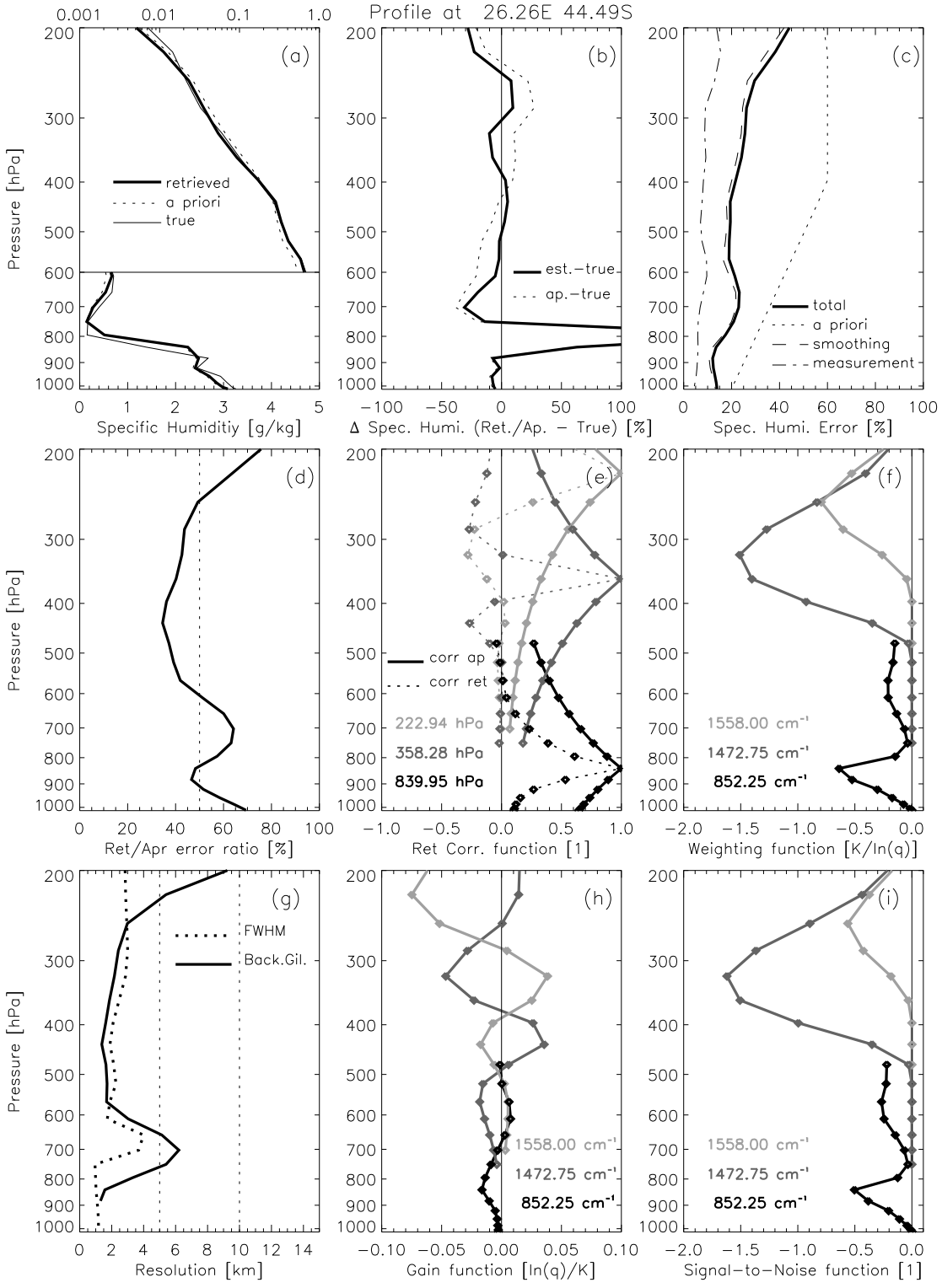

Figure 6: Optimal estimation results for the error analysis and various functions characterizing the retrieval performance (c. f. section 2.3) for a representative mid latitude humidity profile (44.5° S, 26.2° E; c. f. Figure 2). For clarity, the characterization functions are shown for three representative levels (∼840, ∼360, and ∼220 hPa) and channels (852.25, 1472.75, and 1558.0 cm^{-1}) only. See text for explanation and discussion of the panels.

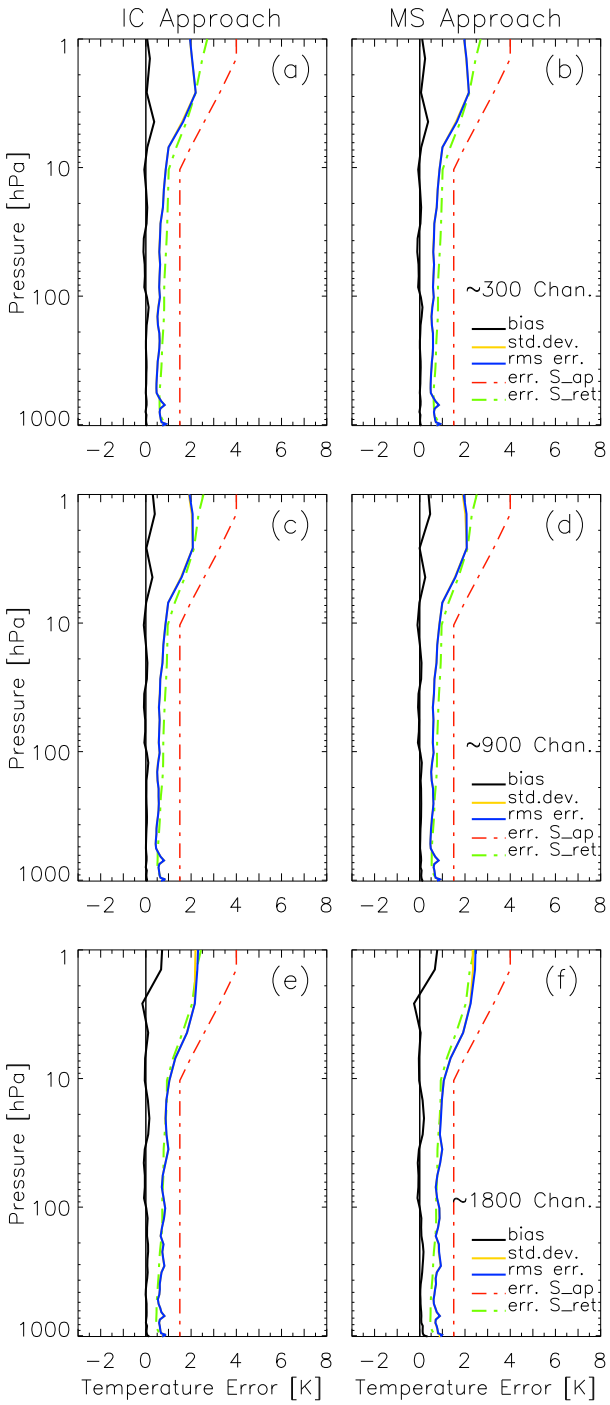

Figure 7: Temperature results of the joint retrieval algorithm for six different retrieval cases (3 channel numbers, each for IC and MS approach). Bias (solid black line), standard deviation (solid gray line), rms error (dashed black line), standard error (square-root of diagonal elements) specified in the *a priori* error covariance matrices (dashed-dotted black line), and the standard error (square-root of diagonal elements) as obtained in the retrieval error covariance matrices (dashed-dotted gray line).

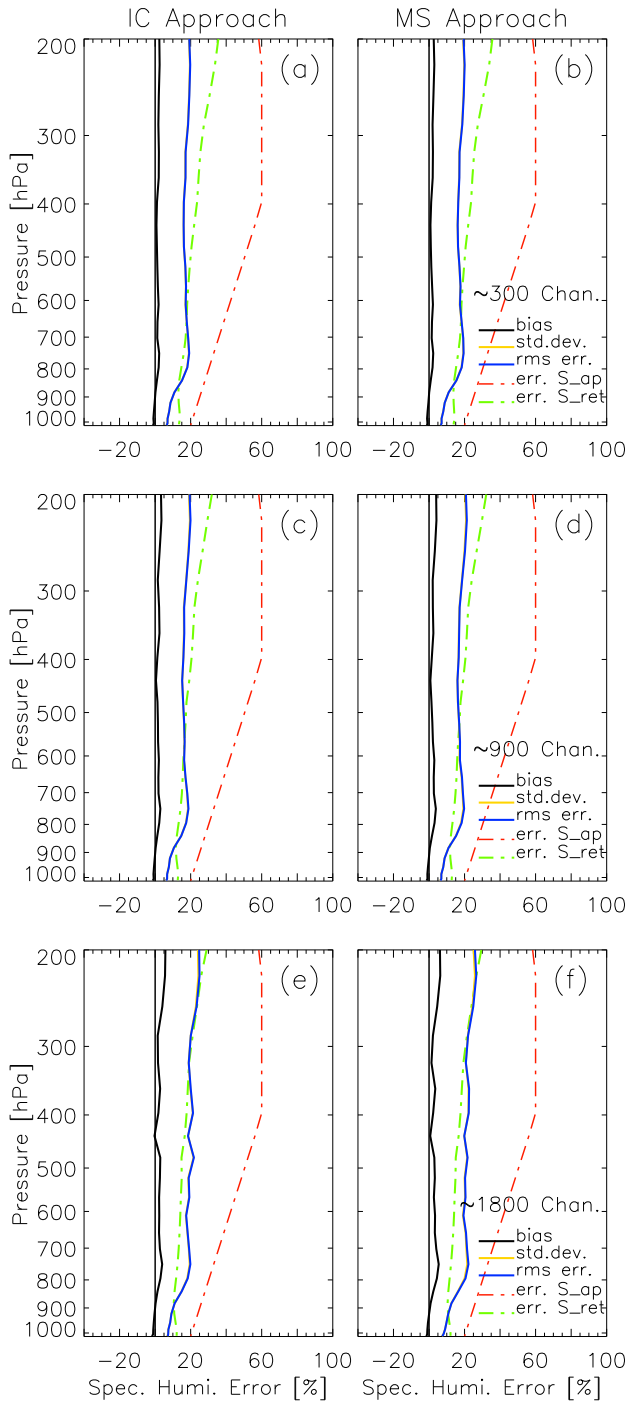

Figure 8: Humidity results of the joint retrieval algorithm for six different retrieval cases (3 channel numbers, each for IC and MS approach). Bias (solid black line), standard deviation (solid gray line), rms error (dashed black line), standard error (square-root of diagonal elements) specified in the *a priori* error covariance matrices (dashed-dotted black line), and the standard error (square-root of diagonal elements) as obtained in the retrieval error covariance matrices (dashed-dotted gray line).

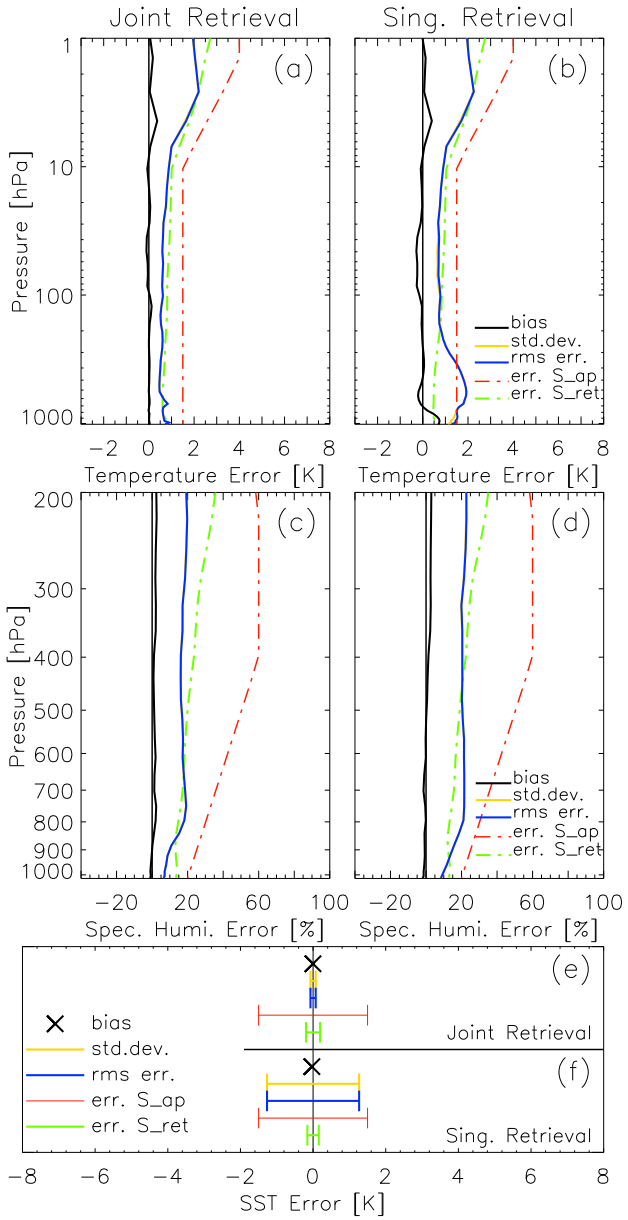

Figure 9: Comparison of the results for multi-parameter retrieval and single-parameter retrievals for temperature (upper panels), humidity (middle panels), and SST (lower panels), respectively. Bias (solid black line; SST: black cross), standard deviation (solid gray line; SST: dark-gray error bars), rms error (dashed black line; SST: solid black), standard error (square-root of diagonal elements) specified in the *a priori* error covariance matrices (dashed-dotted black line; SST: solid light black), and the standard error (square-root of diagonal elements) as obtained in the retrieval error covariance matrices (dashed-dotted gray line; SST: solid light gray).

4 Conclusions and Outook

The present study was based, in terms of forward modeling, on the usage of the fast radiative transfer model RTIASI (*Matricardi and Saunders* (1999)). RTIASI was found to be suitable for the calculation of radiances and Jacobians for temperature, humidity, ozone, and SST for our purpose of a combined temperature, humidity, and ozone profile and SST retrieval from IASI spectra and it provides satisfactory forward model error characteristics.

Since the IASI instrument has more than 8000 channels we implemented channel reduction algorithms since the large computational burden otherwise is neither necessary nor practical in the climatological application we target. A two-step procedure for down-selecting the channels was introduced. The first step includes the removal of channels containing significant contributions from parts of the spectrum not relevant for the retrieval of the atmospheric parameters dealt with here. The second step was the selection of the most informative channels out of the remaining sample.

From two approaches tested, the "information content" (IC) approach and "maximum sensitivity" (MS), approach we found both computationally efficient and robust and leading to similarly good retrieval performance. As still the IC approach performs slightly better, we adapt this as future baseline. Investigating by how much the total number of 8461 IASI channels can be reduced without appreciable decrease in retrieval performance we found that ∼300 channels (∼3.5% of total) is sufficient, enabling a computationally very fast processing.

The solution of the inverse problem was implemented via a joint optimal estimation scheme for temperature, humidity, ozone, and SST. The moderate non-linearity of the radiative transfer problem was taken into account by using an iterative Gauss-Newton type inversion algorithm based on a Taylor series expansion about a first guess (*a priori*) state.

We investigated the retrieval performance of the joint optimal estimation system based on a complete MetOp orbit of simulated IASI data (∼23 000 spectra):

In general we found that the system provides profiles of temperature and humidity, which improve significantly over the *a priori* profiles from an ECMWF 24h forecast throughout the retrieval domains of interest in the atmosphere. In the case of ozone, improvements were found especially in those stratospheric regions which exhibit high concentrations of this gas, i. e., around the peak of the atmospheric ozone layer, where rms errors were reduced to near 10% over *a priori* errors of 20%. The SST retrieval is found very robust and accurate with rms errors at the 0.1 K level, essentially independent of *a priori* information.

Weaknesses in retrieving atmospheric parameters occur at levels where the sensitivity of the relevant weighting functions in the Jacobian matrix is limited, such as in the case of temperature in the upper stratosphere, in the case of humidity in the lower troposphere (e. g., top of boundary layer gradients) and in the stratosphere (no reasonable sensitivity), and in the case of ozone in regions of not sufficiently high concentrations of ozone. The sensitivity to SST is overall very good, thanks due to the "atmospheric window" channels.

Quantifying more closely temperature and humidity accuracy and vertical resolution, we found that the processing system robustly retrieves tropospheric and lower stratospheric temperature to 0.5–1 K accuracy, at ∼2–10 km vertical resolution. Tropospheric specific humidity is retrieved to 15–20% accuracy (<15% below 850 hPa) with ∼1.5–3 km vertical resolution. The coarse temperature resolution from formal estimates (Averaging Kernel full-widths at half maximum and Backus-Gilbert measures) is due to relaxed humidity *a priori* error specifications for strengthening *a priori* independence of the retrieved data. In general the performance is similar to the one reported by other authors (e. g., *Collard* (1998)) based on independent algorithms.

Detailed insight into retrieval system performance properties was also obtained from formal error analysis and characterization where we discussed in this report retrieval error correlation, retrieval-to-apriori error ratio, as well as weighting, gain, and signal to noise functions.

In comparing the joint multi-parameter retrieval to simplified single-parameter retrievals it was clearly found that the joint processing significantly improves over the single-parameter retrieval. While this provided no surprise in itself, these evaluations represented a strong further test and verification of the new retrieval system and provided us with solid confidence in its robustness and utility for future large-scale application.

The results obtained in this report provided guidance for the currently ongoing advancements, including a further improvement of the statistical model of the *a priori* uncertainties for temperature and humidity as well as the usage of the newest version of the forward model RTIASI, which contains a new scheme for prediction of the water vapor continuum, a refinement of the vertical pressure grid, an inclusion of some more trace gases as profile variables, an introduction of a solar term to evaluate the solar radiance reflected by a land or water surface (c. f. *Matricardi* (2003)) and an inclusion of clouds and aerosols (*Matricardi* (2004)). The finalized updated processing system will include a cloudy profiles elimination step.

The system is scheduled to process MetOp IASI data into climatologies with particular interest in middle and upper troposphere moisture changes along with changes in SST and the thermal structure of the troposphere. As this report indicates, the IASI data hold high potential to significantly improve upon current operational meteorological satellite data for these purposes.

Acknowledgments

The authors thank J. Fritzer, A. K.Steiner (WegCenter, Univ. of Graz, Austria), C. Retscher (ESA/ESRIN, Frascati, Italy), and A. Loescher (DMI, Copenhagen, DK) for many valuable discussions and advice during the processing system development, E. Weisz (SSEC, Univ. of Wisconsin, Madison, WI, USA) for fruitful discussions on retrieval methodology, P. Schluessel (EUMETSAT, Darmstadt, Germany) for providing the forward model RTIASI (which is a property of EUMETSAT) and the IASI level 1c noise values, and M. Matricardi (ECMWF, Reading, U. K.) for helpful advice related to RTIASI. ECMWF provided atmospheric analyses and short term forecast fields. M. Schwaerz and M. Pock received financial support for the work from the MULTICLIM project funded by the Austrian Ministry for Traffic, Innovation, and Technology and managed under Contract No. ALR-OEWP-WV-326/06 of the Austrian Aeronautics and Space Agency (FFG-ALR).

List of References

Camy-Peyret, C., and J. Eyre (1998), The IASI science plan, *ISSWG report*, CNES, Paris, France.

Cayla, F. (1996), Simulation of IASI spectra, *CNES document*, CNES, Paris, France.

Collard, A. D. (1998), Notes on IASI performance, *Forecasting Research Technical Report 256*, The Met. Office, Exeter, U. K.

ECMWF (2004), *IFS Documentation CY28r1*, European Centre for Medium-Range Weather Forecasts, Reading, UK.

Kirchengast, G., J. Hafner, and W. Poetzi (1999), The CIRA86aQ_UoG model: An extension of the CIRA-86 monthly tables including humidity tables and a Fortran95 global moist air climatology model, *Tech. Rep. for ESA/ESTAC No. 8/1999*, IGAM, University of Graz, Austria.

Kirchengast, G., J. Fritzer, and J. Ramsauer (2002), End-to-end GNSS occultation performance simulator version 4 (EGOPS 4) software user manual (overview and reference manual), *Tech. Rep. for ESA/ESTAC No. 3/2002*, IGAM, University of Graz, Austria.

Lavanant, L., and A. C. L. Lee (2005), A global cloud detection scheme for high spectral resolution instruments, in *Proceedings of the Fourteenth International TOVS Study Conference*, pp. 149 – 160, Beijing, China.

Lerner, J. A., E. Weisz, and G. Kirchengast (2002), Temperature and humidity retrieval from simulated Infrared Atmospheric Sounding Interferometer (IASI) measurements, *J. Geophys. Res.*, *107*, 10.1029/2001JD900,254, 4–1 – 4–11.

Liou, K. N. (2002), *An Introduction to Atmospheric Radiation (Second Edition)*, Elsevier Science (USA), Orlando.

Liu, X., T. S. Zaccheo, and J.-L. Moncet (2000), Comparison of different non-linear inversion methods for retrieval of atmospheric profiles, in *Proceedings of the* 10^{th} *Conference of Satellite Meteorology*, pp. 293–295, Long Beach, California.

Matricardi, M. (2003), RTIASI-4, a new version of the ECMWF fast radiative transfer model for infrared atmospheric sounding interferometer, *ECMWF Technical Memorandum*, ECMWF, Research Department, Reading, U. K.

Matricardi, M. (2004), The inclusion of aerosols and clouds in RTIASI, *Tech. Rep. Contract EUM/CO/02/989/PS*, ECMWF, Research Department, Reading, U. K.

Matricardi, M., and R. Saunders (1999), A fast radiative transfer model for simulation of infrared atmospheric sounding interferometer radiances, *J. Appl. Optics*, *38*, 5679–5691.

Press, W. H., B. P. Flannery, S. A. Teukolsky, and W. T. Vetterling (1992), *Numerical Recipes in FORTRAN: The Art of Scientific Computing*, Cambridge University Press, Cambridge.

Rieder, M., and G. Kirchengast (2001), Error analysis and characterization of atmospheric profiles retrieved from GNSS occultation data,, *J. Geophys. Res.*, *106*, 31,755–31,770.

Rodgers, C. D. (1996), Information content and optimization of high spectral resolution measurements, in *Proceedings of SPIE Conference 2830, Optical Spectroscopic Techniques and Instrumentation for Atmospheric and Space Research II*, pp. 136 – 147, Denver.

Rodgers, C. D. (2000), *Inverse Methods for Atmospheric Sounding: Theory and Practice*, World Scientific, Singapore.

Schmetz, J., W. P. Menzel, C. Velden, X. Wu, L. van de Berg, S. Nieman, C. Hayden, K. Holmlund, and C. Geijo (1995), Monthly mean large scale analysis of upper troposphere humidity and wind field divergence derived from three geostationary satellites, *Bull. Amer. Meteor. Soc.*, *76*, 1578 – 1584.

Shannon, C. E., and W. Weaver (1976), *Mathematische Grundlagen der Informationstheorie*, Oldenbourg, München, first published: 1949.

Spencer, R. W., and W. D. Braswell (1997), How dry is the tropical free troposphere? Implications for global warming theory, *Bull. Amer. Meteor. Soc.*, *78*, 1097 – 1106.

Weisz, E. (2001), Temperature profiling by the Infrared Atmospheric Sounding Interferometer (IASI): Advanced retrieval algorithm and performance analysis (Ph. D. thesis), *Scientific Rep. 11*, IGAM, Institute of Physics, University of Graz, Austria.

Weisz, E., G. Kirchengast, and J. A. Lerner (2003), An efficient channel selection method for Infrared Atmospheric Sounding Interferometer data and characteristics of retrieved temperature profiles, *Scientific Rep. 15*, IGAM, University of Graz, Austria.